Design, Fabrication, and Testing of a MEMS Microturbine

Byung Sun Jeon
Research Engineer, Hyundai Motor Company, Jangduk-Dong 772-1, Whasung-Si, Gyunggi-Do 445-706, Korea
Kun Joong Park
Graduate Student, School of Mechanical and Aerospace Engineering, Seoul National University, Shinlim-Dong, Kwanak-Gu, Seoul 151-742, Korea
Seung Jin Song*
Associate Professor, School of Mechanical and Aerospace Engineering, Seoul National University, Shinlim-Dong, Kwanak-Gu, Seoul 151-742, Korea
Young Chang Joo
Assistant Professor, School of Materials Science and Engineering, Seoul National University, Shinlim-Dong, Kwanak-Gu, Seoul 151-742, Korea
Kyoung Doug Min
Associate Professor, School of Mechanical and Aerospace Engineering, Seoul National University, Shinlim-Dong, Kwanak-Gu, Seoul 151-742, Korea

This paper describes the design, fabrication, and testing of a microturbine developed at Seoul National University Here, the term "microturbine" refers to a radial turbine with a diameter on the order of a centimeter Such devices can be used to transmit power for various systems The turbine is designed using a commercial CFD code, and it has a design flow coefficient of 0 238 and work coefficient of 0 542 It has 31 stator blades and 24 rotor blades A hydrodynamic journal bearing and hydrostatic thrust bearings counteract radial and axial forces on the rotor The test turbine consists of a stack of five wafers and is fabricated by MEMS technology, using photolithography, DRIE, and bonding processes The first, second, fourth, and fifth layers contain plumbing, and hydrostatic axial thrust bearings for the turbine The third wafer contains the turbine's stator, rotor, and hydrodynamic journal bearings Furthermore, a turbine test facility containing a flow control system and instrumentation has been designed and constructed In performance tests, a maximum rotation speed of 11,400 rpm and flow rate of 16,000 sccm have been achieved

Key Words : Microturbine, Micro Power System, High Aspect Ratio, DRIE, Si Direct Bonding

Nomenclature

C Chord length
C_p Specific heat of constant pressure
Kn. Knudsen number
L . Characteristic length
M Mach number
P . Pressure
R Gas constant, turbine reaction
s Blade pitch
T Temperature
U . Rotational velocity
V Absolute velocity
V' Relative velocity
v ' Tangential velocity
W Radial velocity

* Corresponding Author,
E-mail sjsong@sun ac kr
TEL +82-2-880-1667, **FAX** +82-2-883-0179
Associate Professor, School of Mechanical and Aerospace Engineering, Seoul National University, Shinlim-Dong, Kwanak-Gu, Seoul 151-742, Korea (Manuscript **Received** May 3, 2004, **Revised** December 20, 2004)

β Blade angle
γ Ratio of specific heat
η_0 Absolute film viscosity
λ Mean free path
Π Dimensionless film pressure $\Pi = p(\Delta h/h)^2/\eta_0\omega$
φ Flow coefficient
ψ Loading coefficient
ω Angular velocity as U over r

Subscripts

a Stator inlet
b Rotor inlet
c Rotor exit
t Total

1. Introduction

Many applications require micro power and propulsion devices Portable electronic devices, outdoor leisure activities, and electronic cooling all require compact mobile power generation systems and micro compression/expansion devices Furthermore, future Micro Air Vehicles (MAV's) and micro satellites will demand compact propulsion devices The LiSO battery BA5590 currently used for radio communication has a specific energy of 170 W-hr/kg, and a hydrocarbon fuel such as butane has a theoretical specific energy of 13,000 W-hr/kg (Shirley, 1998) Assuming 20% efficiency in the energy conversion cycle, a micro power system can offer a potential available specific energy of 2,600 W-hr/kg, or 15 times larger than that of BA5590

To take advantage of such potential, variety of micro power systems are being studied A group at UC Berkeley is developing a Micro Wankel engine (Fernandez-Pello et al, 2003), and Honeywell International & University of Minnesota are investigating a micro free-piston knock engine (Aichlmayr et al, 2002) Ehrich and Jacobson (2001) at MIT has fabricated a microturbine which has attained speeds up to 1,400,000 rpm Also a microcombustor (Mehra et al, 2000) and a compressor driven by an electrostatic motor have been fabricated and tested (Frechette et al, 2001) A Stanford group has tested a micro compressor (Johnston et al, 2003) In Japan, Ishikawajima-Harima Heavy Industries and Tohoku University are developing a larger engine capable of producing hundreds of Watts (Tanaka et al, 2002)

Such micro power systems need to be on the order of cubic centimeters, with a power output of 10-100 Watts, and require manufacturing accuracies on the order of microns One enabling technology is micromachining, capable of making holes on the order of ten microns. However this method is expensive and slow Another option is the Micro Electro-Mechanical System (MEMS) technology which satisfies the precision requirement at reasonable costs Therefore, the MEMS processes have been adopted for fabrication in this study

Since power MEMS is a new field, no established design, fabrication, and testing methods yet exist Therefore, the objective of this research is a broad one — to develop enabling technologies for a microturbine To achieve this, a multidisciplinary team has been assembled at Seoul National University (SNU) This paper is organized as follows After the Introduction, Section Two introduces the microturbine design process Section Three describes the MEMS fabrication methods, including the DRIE and bonding processes Section Four presents test facility design, and Section Five shows the test results Finally, Section Six ends with conclusions

2. Aerodynamic Design

A radial microturbine has been designed using a conventional commercial Navier-Stokes code Before aerodynamic design, a cycle analysis has been carried out Assuming a turbine efficiency of 0 70 (due to increased viscous losses at small scales), turbine inlet/exit pressure ratio of 4 23 and a mass flow rate of 20,000 standard cubic centimeter per minute (sccm) were found to have the best specific work (Table 1) Aerodynamically, the envisioned microturbine is "very small" when compared to the conventional machinery Therefore, one needs to check whether the microturbine can be designed using a continuum ap-

Table 1 Microturbine specifications

Rotation mass flow	20,000 sccm
Efficiency	0 7
Pressure ratio	0 236
Blade number	Stator 31 Rotor 24
Blade angle	Stator inlet 0°, exit 82 4° Rotor inlet 83 8°, exit 7 3°
Blade height	0 2 mm
Reynolds number	11,000
Exit Mach number	0 90
Flow coefficient	0 238
Loading coefficient	0 542
Reaction	0 409

proach For values of Knudsen number, defined as the ratio of the mean free path and the characteristic length $Kn=\lambda/L$ (Kim, 2001. Barber and Emerson, 2002 · Gad-el-Hak, 1999) less than 0 001, a continuum approach (i e Navier-Stokes equation with no-slip boundary conditions) can be used For an ideal gas modeled as rigid spheres, the mean free path is approximately 70 nm for air at atmospheric temperature and pressure The envisioned microturbine has a diameter of 4 1 mm, resulting in Kn values of approximately $1\ 148\times10^{-6}$ Thus, continuum approach was found to be appropriate

Since radial turbomachines are often used at small scale applications, it was assumed from the cycle stage that the compressor and turbine would be of radial type This design choice was mainly dictated by two constraints First, at low flow rates, a radial turbine can deliver more expansion per stage than an axial one (Hill and Peterson, 1992), resulting in higher cycle efficiency. Second, a radial machine is easier to fabricate with MEMS technique which is limited to 2-D geometries

The Euler turbine equation determines the blade inlet and exit angles for the selected pressure ratio (Table 1), and velocity triangles (Fig 1) determine the turbine's characteristic variables as follows For assumed blade angles, upstream stagnation conditions (P_t, T_t), and stator inlet Mach number (M_a), isentropic relations (Eq (1))

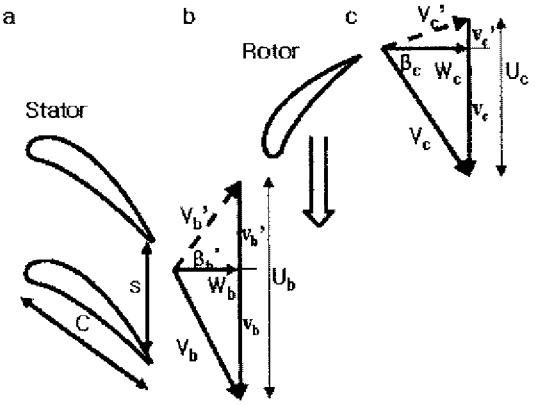

Fig. 1 Turbine velocity triangles

$$P=\frac{P_t}{\left(1+\frac{\gamma-1}{2}M_a^2\right)^{\frac{\gamma}{\gamma-1}}},\quad T=\frac{T_t}{\left(1+\frac{\gamma-1}{2}M_a^2\right)},\quad V=M\sqrt{\gamma RT} \tag{1}$$

can be used to determine velocity triangles at stator inlet (Station a), rotor inlet (Station b), and rotor exit (Station c) Next, the following equations (Eqs (2) ~ (4))

$$\text{Flow coefficient } \Phi=\frac{\overline{W}}{U_{tip}}\approx\frac{W_a+W_b+W_c}{3U_{tip}} \tag{2}$$

$$\text{Loading coefficient } \psi=\frac{C_p\Delta T_t}{U_{tip}^2} \tag{3}$$

$$\text{Reaction } R=\frac{V_c'^2-V_b'^2}{(V_c'^2-V_b'^2)+(V_b'^2-V_a'^2)} \tag{4}$$

are used to obtain turbine flow coefficient, loading coefficient, and reaction The flow coefficient is the ratio of radial velocity to turbine's rotational speed and indicates mass flow rate through the machines The loading coefficient indicates how much enthalpy change occurs across turbine, and the reaction is the ratio of the pressure drop across the rotor divided by the pressure drop across both stator and rotor For the selected design case, the corresponding values are 0 238, 0 542, and 0 409, respectively (Table 1) Solidity, or the ratio of the chord length C to pitch s (Fig 1), is another important design parameter and is determined by the number of blades. For the SNU turbine, 31 stator blades and 24 rotor blades were selected These blade numbers are

higher than the 24 stator blades and 20 rotor blades selected by MIT (Ehrich and Jacobson, 2001). Thus, the SNU turbine has higher solidity than MIT and this design choice was made to alleviate flow separation problems which can occur in machines with lower solidity.

Detailed blade design has been carried out with a commercial code CFX-TASCflow. For structural considerations, a maximum blade height of 0.2 mm was selected because it is about half of the silicon wafer thickness (450 μm). Non-uniform grid distribution was adopted, and cyclic boundary conditions were used. Effort was made to prevent flow separation, especially on the suction side of the blade, and this resulted rather "thick" blades. Figure 2(a) shows the overall view of the designed turbine including the stator and rotor blades, and Fig. 2(b) shows the velocity distribution at the mid-span of a stator blade.

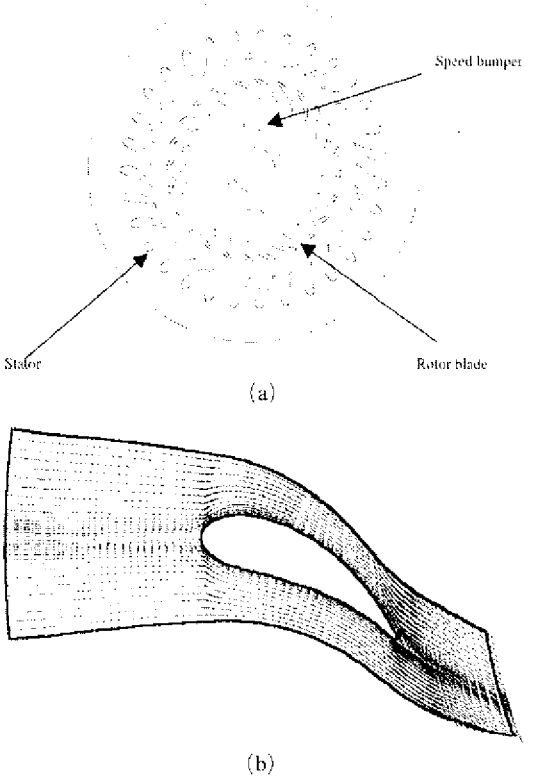

Fig. 2 Microturbine design : (a) Microturbine rotor and stator, (b) Velocity distribution at mid-span around a microturbine stator

The microturbine bearings need to withstand high-speeds need a long fatigue life time, and require low noise level. Therefore, self-acting fluid film gas bearings have been selected (Hamrock, 1994). To support the rotor, the microturbine has a hydrodynamic journal bearing and hydrostatic thrust bearings. Also, such gas bearings enhance system simplicity (Stolarski, 2000), and facilitate fabrication with MEMS process. A 2-dimensional Reynolds equation using Alternating Direction Implicit (ADI) method has been need for bearing analysis, and the bearing specifications are given in Table 2.

The entire test turbine consists of five layers of wafer. Wafer No. 3 contains the microturbine rotor (Fig. 3). Wafers No. 1 and 5 have inlet/outlet ports for the main microturbine flow, thrust

Table 2 Pressure and force in the journal bearing

Non-dimensional pressure	Pressure	Force
8.48×10^{4}	102 kPa	1.3×10^{3} N

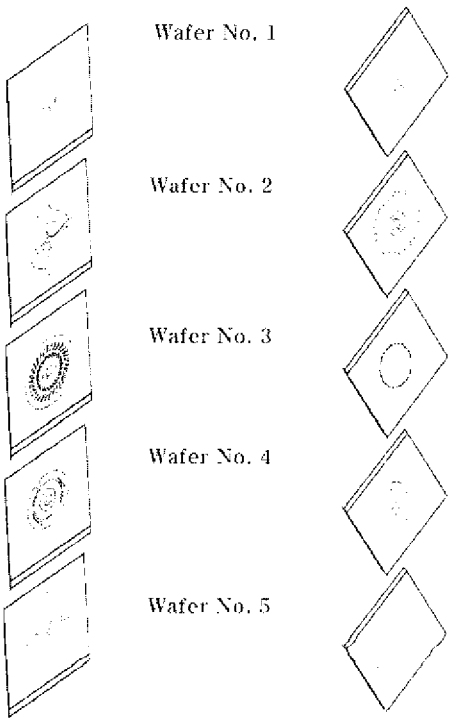

Fig. 3 Top and bottom views of the five wafers of microturbine (15 mm×15 mm×2.25 mm)

bearing, and journal bearing. Wafers No. 2 and 4 transport the inflow fluid to thrust and journal bearings.

3. Fabrication Process

MEMS fabrication technology is based mostly on etching of silicon (Si). From structural considerations, silicon is attractive because of its high strength, and, therefore, Si wafers have been used to construct the microturbine. In all, five wafers need to be double-side-polished (DSP) and fabricated separately using a continuous process flow. In all, the microturbine fabrication requires 11 masks, and complicated processes of more than 100 steps. The process flow is shown in Fig. 4.

Next two sections introduce two particular fabrication challenges, which arise specifically in the fabrication of the microturbine — Deep Reactive Ion Etching (DRIE) and three-dimensional integration of wafers.

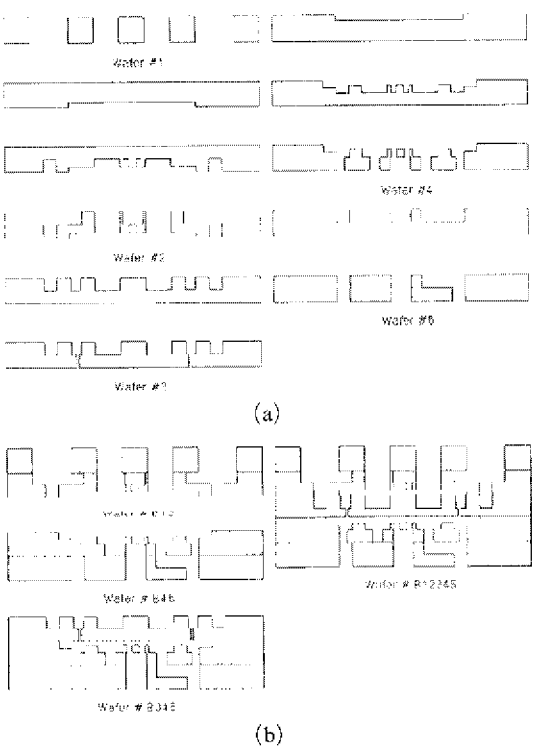

Fig. 4 Microturbine fabrication process flow: (a) wafer etching process, (b) wafer bonding process

3.1 DRIE for high aspect ratio geometry

This section describes two fabrication techniques which have been newly developed by the authors — a 5-3-6 procedure and the use of aluminum barrier. In general, MEMS need etching depths of only a few microns. However, microturbine requires geometries with aspect ratios (depth/width) greater than 10. For example, the journal bearing has a depth of 300 microns and a width of 30 microns, or an aspect ratio of 10. To etch such a geometry, a technique known as DRIE is needed (Ayon et al., 1999). For this study, a 5-3-6 step has been newly used to make a high aspect ratio structure. 5 seconds is the time for polymer passivation; 3 seconds is the time for polymer deposition on bottom; and 6 seconds is the time for etching. This step maintains a vertical structure as well as that of 5-3-5 step, but the etching rate of this step is 11% faster than that of the conventional 5-3-5 step. Also 5-3-6 process decreases the number of a scalloping, and the authors believe that 5-3-6 process is better suited for deep etching than the conventional 5-3-5 process.

Also, wafers require backside through etching after frontside etching, and a barrier that prevents the argon coolant from leaking during DRIE process is needed. Generally, barrier for through etching is made of quartz wafer. However, the use of quartz wafer causes microloading effect such as severe pitting on the backside surface of the Si wafer and requires long process time due to the additional debonding step. To overcome these problems, the authors have invented the use of thin Al film to bond the quartz wafer as the backside barrier. Al film prevents the microloading effect by eliminating ion scattering. Moreover, Al film deposition is used widely and decreases the process time. Thus, in this study, a new method using Aluminum barrier has been developed. Figures 5(a) and (b) show rotor blades and stator blades in Wafer No. 3. Vertical lines shown Fig. 5(b) are due to non-smooth mask lines and particles.

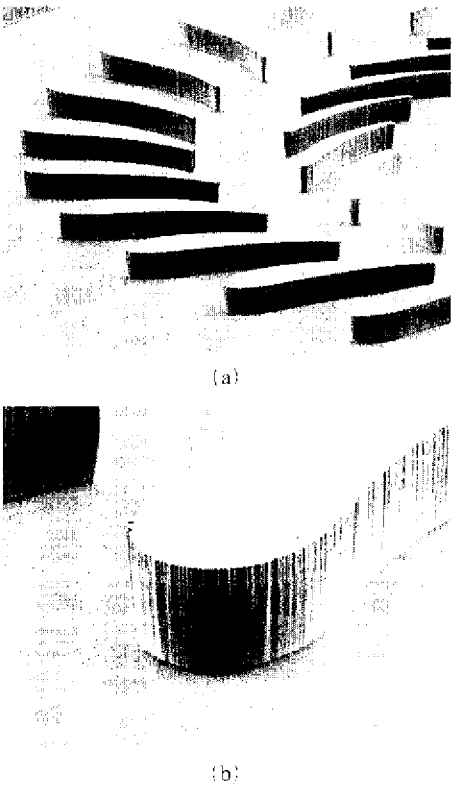

Fig. 5 Turbine wafer fabrication results: (a) Turbine stator and rotor blades, (b) Rotor blade in Wafer No. 3

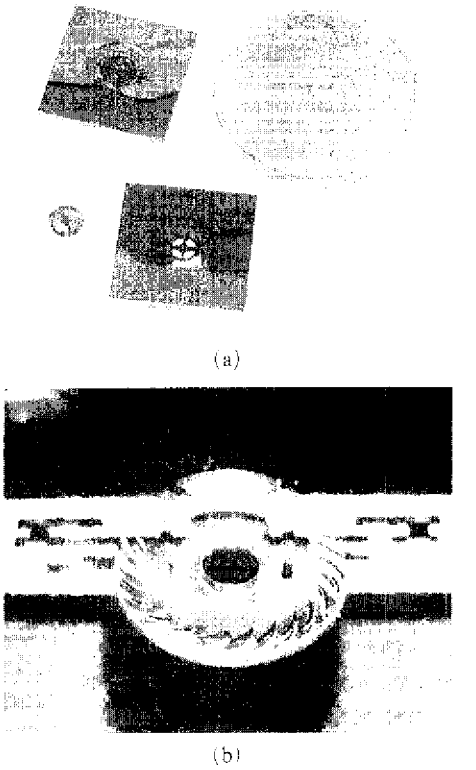

Fig. 6 Photographs of microturbine

3.2 Three dimensional integration process

The etching process is a two dimensional technique. Therefore, to build a three-dimensional structure, one has to stack layers of two-dimensional wafers. To do so, alignment and bonding need to be carried out. Alignment refers to precise stacking of wafers. To prevent mismatching, alignment keys can have been etched onto wafers and used for positioning. Each wafer is aligned using an EV620 bonding aligner and an EV 501 bonder.

Aligned wafers are bonded by silicon-to-silicon direct bonding process. First, silicon wafers are cleaned via Sulfuric-Peroxide Mixture (SPM) and RCA methods*. SPM cleaning, or piranha cleaning, uses a 4 : 1 mixture of sulfuric acid (H_2SO_4) and hydrogen peroxide (H_2O_2) to remove organic particles. RCA cleaning uses a 1 : 1 : 5 mixture of sodium hydroxide (NH_4OH), hydrogen peroxide (H_2O_2), and deionized water to remove metallic contaminants. Since contamination reduces bonding strength, strict cleaning process control is needed. After aligning and pre-bonding, the bonded wafers are annealed at 1100℃ for 1 hour before a final SPM cleaning.

Fig. 6 shows the final result. The microturbine has dimensions of 15 mm×15 mm×2.25 mm. Fig. 6(a) shows the rotor with 4.1 mm diameter, the lower bearing part, and the upper bearing part along with a 100 Won coin. Figure 6(b) shows an oblique view of a microturbine with all the flow passages.

4. Turbine Test Facility

The microturbine test facility consists of test section packaging, flow control system, and speed measurement system as shown Fig. 7. The test section packaging has dimensions of 100 mm×30 mm×18.3 mm, and has 3 plates. The upper and

*RCA cleaning refers to a method developed by Werner Kern at RCA Laboratories in the late 1960's

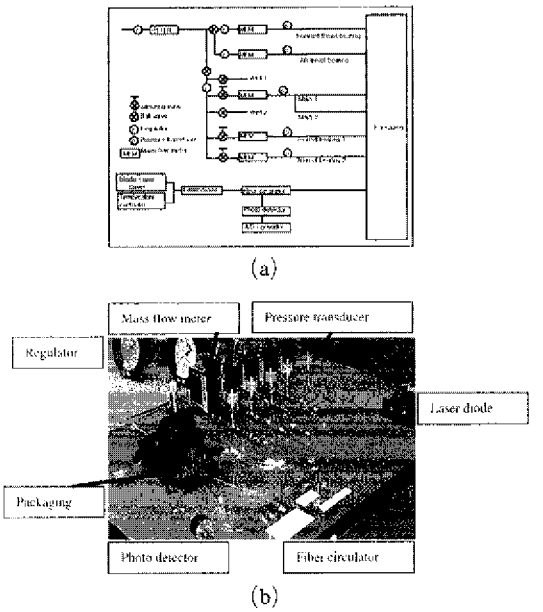

(a)

(b)

Fig. 7 Microturbine test facility : (a) Schematic and (b) Picture

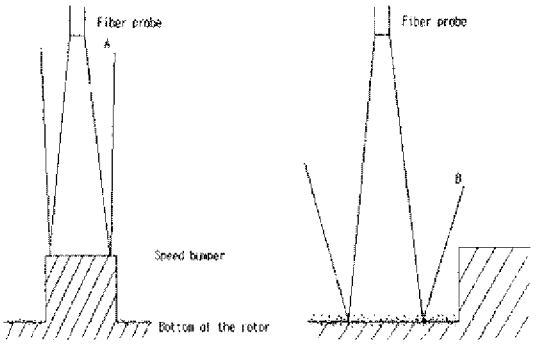

(a) Speed bumper surface (b) Rotor surface

Fig. 8 Laser signal pick up from the rotor speed bumper

Table 3 Test instrument

Mass flow meter	MKS 179A
Pressure transducer	Druck PMP 1400
Regulator	Omega PRG101
Laser diode	Thorlabs pigtailed 1550 nm, 1.5 mW
Photo detector	Thorlabs PDA400
Fiber circulator	JDSUniphase CR5500
A/D converter	NI PCI-MIO-16E-1

lower acrylic plates are transparent to the visible light, and they have 8 fluid inlet/outlet ports. The 8 ports include 2 main inlet fluid ports, 4 thrust bearing inlet and outlet ports, and 2 journal bearing inlet ports. The upper plate also has ducts for turbine exhaust, the fiber probe of the speed sensor. The middle steel plate contains microturbine. Compressed nitrogen gas is the working fluid and it is filtered to remove particles greater than 0.1 μm.

Flow control system regulates pressure and mass flow rate through each component. The flow in the thrust bearing is low at high pressure. The main flow has a high flow rate at low pressure. Therefore, the two flows are regulated separately. The main turbine flow and the journal bearing flow are controlled together while the thrust bearing flow is done independently. All ports are connected to 10 bar pressure transducers with a 0.3% accuracy and 1,000, 2,000, and 20,000 sccm mass flow meters with an accuracy of 1%. Finally, pressure is regulated manually.

The speed is measured by the change of the intensity of the beam reflected from the speed bumper on the rotor. The shape and the position of the speed bumper are shown in Fig. 8. The top surface of the speed bumper is mirror smooth because it has the original polished wafer surface. The rotor surface, however, is rougher than the speed bumper due to DRIE etching. As shown in Fig. 8, the beam is mostly reflected from the smooth speed bumper surface, but gets diffused by the coarse rotor surface. Such intensity difference in the reflected light can be measured with a laser probe to determine turbine speed.

The speed measurement system includes a 1.5 mW pigtailed diode laser with a wave length of 1550 nm, a photo detector with a 0.9 A/W sensitivity and a 1.5×10^6 V/A gain, a fiber circulator, and a laser position adjustment device to locate a fiber probe. The beam emitted by the diode laser is controlled by current and temperature controllers. The beam through a fiber circulator is reflected by the speed bump on the rotor, and the reflected beam is detected by a photo detector. A fiber circulator with 3 probes can transmit both sides. Individually 3 probes are connected to a pigtailed diode laser, a photo

detector, and a speed measurement fiber. A laser position adjustment device has 3 micrometers with 0.01 mm step, and controls x, y, and z axis.

All of the data- 5 mass flow meter signals, 5 pressure transducer signals, and 1 photo detector signal- are then digitized via an A/D converter. Sensors used in the test facility are listed in Table 3.

5. Performance Test Results

Figure 9 shows the main turbine mass flow rate plotted vs. time. Initially, the mass flow increases gradually from 0 sccm. This gradual increase is necessary to carefully balance the upper and lower thrust bearings. Finally, the main turbine mass flow rate reaches 16,000 sccm which is about 80% of the designed mass flow rate. At the same time, the main flow pressure increases from 0 bar to 1.8 bar gage pressure. The steps shown in Fig. 9 are due to the manual operation. While increasing turbine rpm, it is important to balance the upper and lower thrust bearings to maintain vertical stability of the rotor. All the flow adjustments are done manually, and the steps are generated during this process.

The mass flow of the journal bearing remains below 180 sccm or about 1.1% of the maximum turbine mass flow rate. The mass flow of the lower thrust bearing is set at 300 sccm, or 1.9% of that of the maximum main fluid, and its pressure is fixed at 1.0 bar gage pressure. The mass flows of all bearings add up to approximately 6% of the main turbine flow. The pressure of the upper thrust bearing, however, is increased continuously with increasing main flow. Figure 10 shows a graph of upper thrust bearing pressure vs. time. Maintaining upper thrust bearing pressure schedule is important for stable rotor operation, and that failure to control upper thrust bearing can cause the turbine rotor to crash into the upper casing.

Fast Fourier Transform (FFT) of the laser signal is plotted versus frequency in Fig. 11. Figure 11 shows a peak at 380 Hz and rest are noise. Since two speed bumpers go by the sensor for every rotation, the maximum rotation speed of the rotor is 190 Hz, or 11,400 rpm. This speed is well below the desired speed of about one million

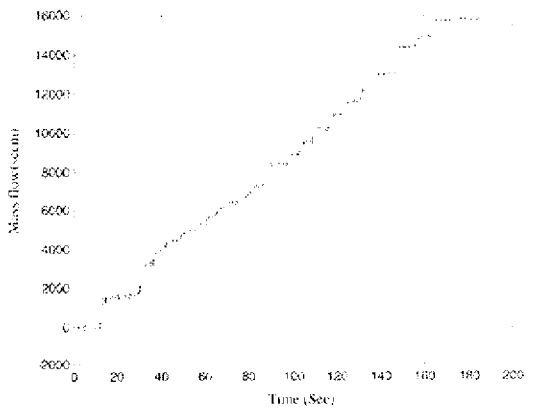

Fig. 9 Microturbine main mass flow rate versus time

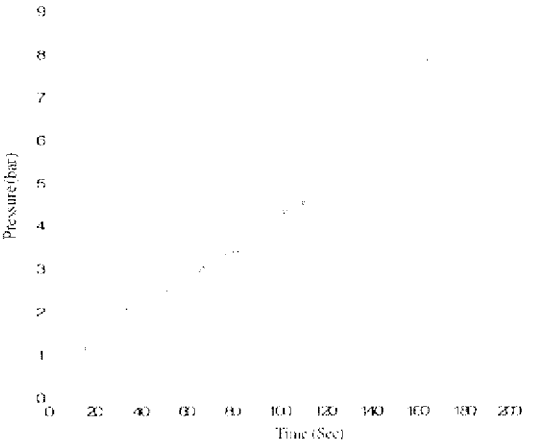

Fig. 10 Upper thrust bearing pressure versus time

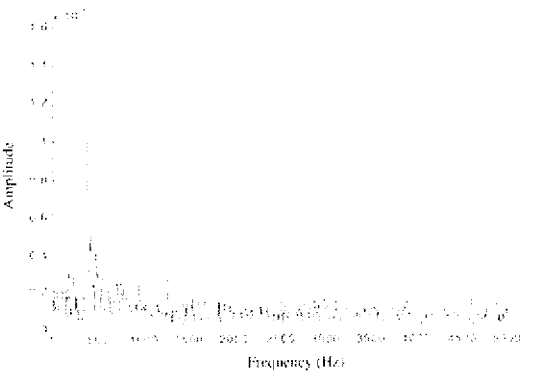

Fig. 11 FFT of microturbine's rotation signal

rpm, and two possible causes are either a thrust bearing failure or a journal bearing failure In Fig 10, the upper thrust bearing pressure increases to 8 bars though the lower thrust bearing is maintained at 1 bar The upper thrust bearing pressure was increased to maintain upper thrust bearing's mass flow rate This pressure difference could have caused the rotor to crash into either upper or lower wafer. Second, imbalance is likely to exist in the rotor due to manufacturing inaccuracies, and the imbalance could cause the rotor to crash into the side wall causing journal bearing failure Efforts are under way to enhance rotor stability and increase operating speed

6. Conclusions

This paper describes the microturbine that has been designed, fabricated, and tested at Seoul National University Contributions of this paper include the following

(1) A microturbine design process has been developed The process includes a thermodynamic cycle analysis, preliminary blade design using one dimensional modeling, and detailed blade design using a Navier-Stokes code For bearing design, Reynolds lubrication equation has been used

(2) Silicon wafer based fabrication capability has been achieved Etching, DRIE, and bonding processes have been developed to successfully fabricate a microturbine Especially, in through etch, the use of 0 7 μm Al film as the backside barrier has been newly developed to prevent pitting of the quartz barrier

(3) A test facility and instrumentation techniques for rotational speed, mass flow rate, and pressure measurement have been developed Using this facility, a maximum operating speed of 11,400 rpm has been achieved

Acknowledgments

The authors acknowledge financial support from the UNITEF and the Micro Thermal System Research Center of the Korea Science and Engineering Foundation

References

Aichlmayr, H T, Kittelson, D B and Zachariah, M R, 2002, "Micro-Homogeneous Charge Compression Ignition (HCCI) Combustion Investigations Employing Detailed Chemical Kinetic Modeling and Experiments," *the Western States Section of the Combustion Institute*, Spring Technical Meeting, La Jolla, CA, 26

Ayon, A A, Braff, R, Lin, C C, Sawin, H H and Schmidt, M A, 1999, "Characterization of a Time Multiplexed Inductively Coupled Plasma Etcher," *Journal of the Electrochemical Society*, Vol 146, No 1, pp 339~346

Barber, R W and Emerson, D R, 2002, "The Influence of Knudsen Number on the Hydrodynamic Development Length within Parallel Plate Micro-Channels," WIT Press, Southampton, UK, *Advances in Fluid Mechanics IV*, pp 207~216

Ehrich, F F and Jacobson, S A, 2001, "Development of High-Speed Gas Bearings for High-Power-Density Micro-Devices," *ASME Turbo Expo 2001*, 2001-GT-0478

Fernandez-Pello, C, Liepmann, D and Pisano A, 2003, MEMS Rotary Combustion Laboratory, University of California at Berkeley http //www me berkeley edu/mrcl

Frechette, L F, Nagle, S F, Ghodssi, R, Umans, S D, Schmidt, M A and Lang, J H, 2001, "An Electrostatic Induction Micromotor Supported on Gas-Lubricated Bearings," *IEEE 14th International Micro Electro Mechanical System Conference*, MEMS 2001, Interlaken, Switzerland

Gad-el-Hak, M, 1999, "The Fluid Mechanics of Microdevices — The Freeman Scholar Lecture," *Journal of Fluids Engineering*, Vol 121, pp 5~33

Hamrock, B J, 1994, *Fudamentals of Fluid Film Lubrication*, McGraw-Hill, Inc, pp 12~23, and 329~330

Hill, P G and Peterson, C R, 1992, *Mechanics and Thermodynamics of Propulsion*, 2nd Ed, Addison-Wesley Publishing Company, Inc, pp 367~370

Johnston, J P, Kang, S, Arima, T, Matsunaga, M, Tsuru, H and Prinz, F B, 2003, "Performance of a Micro-Scale Radial-Flow Compressor Impeller Made of Silicon Nitride," *International Gas Turbine Congress 2003 Tokyo*, OS-110

Kim, H, Won, C S, Jeong, S. and Hur, N, 2001, "Flow Characteristics in a Microchannel Fabricated on a Silicon Wafer," *Transactions of the Korean Society of Mechanical Engineers*, B, Vol 25, No 12, pp 1844~1852 (in Korea)

Mehra, A, Zhang, X, Ayon, A. A, Waitz, I A, Schmidt, M A and Spadaccini, C M, 2000, "A Six-Wafer Combustion System for a Silicon Micro Gas Turbine Engine," *Journal of Microelectromechanical Systems*, Vol 9, No. 4

Shirley, G. B, 1998, "An Experimental Investigation of a Low Renolds Number High Mach Number Centrifugal Compressor," M. S. dissertation, MIT, Cambridge, Massachusetts

Stolarski, T A., 2000, *Tribology in Machine Design*, Butterworth Heinemann, pp 210~212

Tanaka, S, Isomura, K, Kato, T, Sato, F Oike, M, Genda, T, Iiichi, M, Murayama, M, Nakahash, K, and Esashi, M, 2002, "Design and Fabrication Challenges for Micromachined Gas Turbine Generators," *the 9th International Symposium on Transport Phenomena and Dynamics of Rotating Machienery*, Honolulu, Hawaii